

An Experimental and Theoretical Study on the Formation of 2-Methylnaphthalene ($C_{11}H_{10}/C_{11}H_3D_7$) in the Reactions of the Para-Tolyl (C_7H_7) and Para-Tolyl-d7 (C_7D_7) with Vinylacetylene (C_4H_4)

Dorian S. N. Parker,[†] Beni B. Dangi,[†] Ralf I. Kaiser,^{*,†} Adeel Jamal,[‡] Mikhail N. Ryazantsev,^{‡,§} Keiji Morokuma,^{*,‡,||} André Korte,[⊥] and Wolfram Sander[⊥]

[†]Department of Chemistry, University of Hawaii at Manoa, Honolulu, Hawaii 96822, United States

[‡]Department of Chemistry and Cherry L. Emerson Center for Scientific Computation, Emory University, Atlanta, Georgia 30322, United States

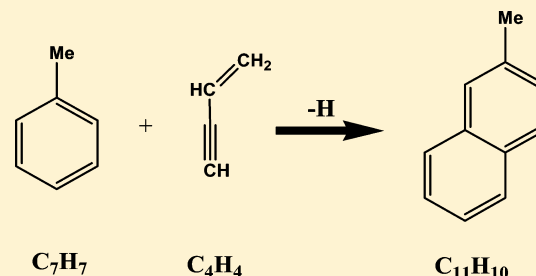
[§]St. Petersburg Academic University Nanotechnology Research and Education Center RAS, St. Petersburg, Russia

^{||}Fukui Institute for Fundamental Chemistry, Kyoto University, Sakyo, Kyoto 606-8103, Japan

[⊥]Faculty of Chemistry and Biochemistry, Ruhr Universität Bochum, Universitätsstraße 150, 44801 Bochum, Germany

S Supporting Information

ABSTRACT: We present for the very first time single collision experimental evidence that a methyl-substituted polycyclic aromatic hydrocarbon (PAH)—2-methylnaphthalene—can be formed without an entrance barrier via indirect scattering dynamics through a bimolecular collision of two non-PAH reactants: the para-tolyl radical and vinylacetylene. Theory shows that this reaction is initiated by the addition of the para-tolyl radical to either the terminal acetylene carbon (C^4) or a vinyl carbon (C^1) leading eventually to two distinct radical intermediates. Importantly, addition at C^1 was found to be *barrierless* via a van der Waals complex implying this mechanism can play a key role in forming methyl substituted PAHs in low temperature extreme environments such as the interstellar medium and hydrocarbon-rich atmospheres of planets and their moons in the outer Solar System. Both reaction pathways involve a sequence of isomerizations via hydrogen transfer, ring closure, ring-opening and final hydrogen dissociation through tight exit transition states to form 2-methylnaphthalene in an overall exoergic process. Less favorable pathways leading to monocyclic products are also found. Our studies predict that reactions of substituted aromatic radicals can mechanistically deliver *odd-numbered* PAHs which are formed in significant quantities in the combustion of fossil fuels.



1. INTRODUCTION

As early as 1927, alkyl-substituted polycyclic aromatic hydrocarbons (PAHs) such as 2-methylnaphthalene were identified as products of hydrocarbon combustion processes.¹ Today, it has been well established that methyl-substituted PAHs are formed during the incomplete combustion of fossil fuel,^{2–6} having received considerable attention in recent decades due to their muta-⁷ and carcinogenic properties.⁸ In extraterrestrial settings, the ubiquitous presence of PAHs together with their (de)hydrogenated, ionized, and protonated counterparts has been inferred from the diffuse interstellar absorptions bands (DIBs)—discrete absorption features superimposed on the interstellar extinction curve ranging from the blue part of the visible (400 nm) to the near-infrared (1.2 μm)^{9,10}—and the unidentified infrared emission (UIE) bands (3 to 14 μm).¹¹ In the interstellar medium, PAHs and related species are suggested to constitute up to 10% of the interstellar carbon budget and have been proposed as the missing link between small carbon clusters and amorphous carbon particles eventually leading to carbonaceous dust grains. However, a persistent debate has

emerged on the role of aliphatic over aromatic carbon–hydrogen (C–H) stretches describing the broad 3.4 μm (2491 cm^{-1}) feature^{12–15} with methyl-substituted PAHs as potential candidates.^{14,16} Here, methyl-substituted naphthalenes—1-methylnaphthalene and 2-methylnaphthalene—provide both aliphatic and aromatic properties. Note, a range of mono-, di-, and trisubstituted methylnaphthalenes and methylphenanthrenes have also been detected in carbonaceous chondrites, thus proposing extraterrestrial origins.^{17–19}

The abundance of PAHs in both terrestrial and extraterrestrial settings can be understood in terms of their inherent thermodynamic stability as derived from their aromaticity compared to their non-PAH counterparts, with a molecule of a molecular formula $C_{10}H_8$ in its non-PAH form such as 1-phenyl-vinylacetylene holding an enthalpy of formation of 220 kJ mol^{-1} higher than the corresponding PAH isomer

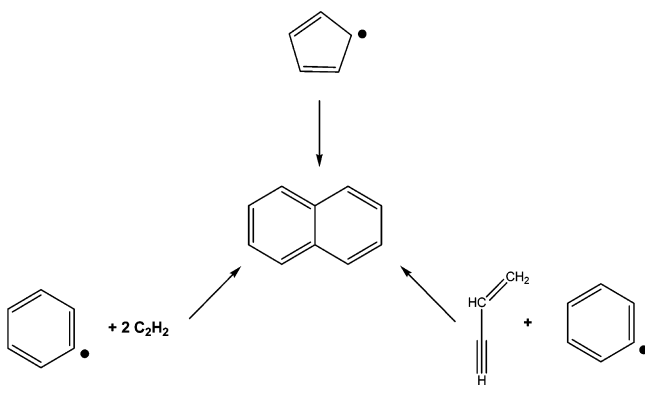
Received: February 3, 2014

Revised: March 12, 2014

Published: March 19, 2014

naphthalene.²⁰ The formation of the prototype PAH with two six-membered rings—naphthalene—has been proposed through the hydrogen abstraction–acetylene addition mechanism (HACA)^{21,22} and adaptations thereof,²³ through the self-reaction of cyclopentadienyl radicals,^{24,25} and via the barrierless reaction of vinylacetylene (HCCC_2H_3) with the phenyl radical (C_6H_5)^{20,26} (Scheme 1). In the present investigation we apply

Scheme 1. Reaction Pathways to Formation of a Prototype PAH; Naphthalene



the latter reaction mechanism to investigate the formation routes to methylsubstituted PAHs through the use of methyl-substituted aromatic radicals.

A recent investigation into the self-recombination of phenyl radicals and the phenyl radical additions to acetylene revealed PAH formation, but not methyl-substituted PAH formation directly.²⁷ Here, we propose a novel route to form methyl-substituted naphthalene via reactions of para-tolyl radical ($\text{C}_6\text{H}_4\text{CH}_3$) with vinylacetylene ($\text{HC}\equiv\text{C}-\text{CH}=\text{CH}_2$). We show that this overall exoergic reaction goes through intermediates and a sequence of isomerization reactions, followed by atomic hydrogen loss to produce 2-methylnaphthalene via a barrierless single collision event in the gas phase.

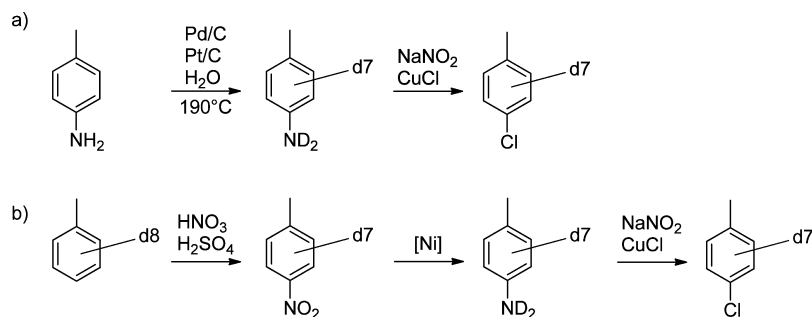
2. EXPERIMENTAL METHOD AND ANALYSIS

The reaction of the para-tolyl radical ($\text{C}_6\text{H}_4\text{CH}_3$; X^2A_1) and of the para-tolyl-d7 radical ($\text{C}_6\text{D}_4\text{CD}_3$; X^2A_1) with vinylacetylene ($\text{CH}_2=\text{CH}-\text{C}\equiv\text{CH}$, X^1A') was conducted under single collision conditions exploiting a universal crossed molecular beam machine.²⁸ Briefly, a supersonic beam of para-tolyl radicals seeded in helium (99.9999%; Gaspro) at fractions of 0.2% was prepared by single photon dissociation of para-chlorotoluene ($\text{C}_7\text{H}_7\text{Cl}$, 98%, Aldrich; $\text{C}_7\text{D}_7\text{Cl}$, 98%; Bochum group) in the primary source chamber. Power dependent

studies suggest that, under our experimental conditions, the barrier of isomerization from para- to the meta-tolyl radical of 260 kJ mol^{-1} cannot be overcome.²⁹ Briefly, helium gas at a pressure of 1,300 Torr was passed through para-chlorotoluene stored at 295 K in a stainless steel bubbler. The gas mixture was released by a Proch-Trickl pulsed valve operating at 120 Hz delayed by $1872 \mu\text{s}$ after the time zero trigger; para-chlorotoluene ($\text{C}_7\text{H}_7\text{Cl}$, $\text{C}_7\text{D}_7\text{Cl}$) was then photodissociated by focusing 10 mJ per pulse of the 193 nm output of a Excimer laser (ComPex 110, Coherent) 1 mm downstream of the nozzle to a spot size of 1 mm by 3 mm. A four-slot chopper wheel located after the skimmer selected a part of the para-tolyl beams ($\text{C}_7\text{H}_7\text{Cl}$, $\text{C}_7\text{D}_7\text{Cl}$) with peak velocities (v_p) of $1550 \pm 30 \text{ ms}^{-1}$ and $1613 \pm 24 \text{ ms}^{-1}$, and a seed ratio (S) of 12.0 ± 0.4 and 12.0 ± 0.3 , respectively. The radical beam was perpendicularly intersected in the interaction region of the scattering chamber by a second pulsed molecular beam of 5% vinylacetylene seeded in argon gas (99.9999%; Gaspro) ($v_p = 626 \pm 20 \text{ ms}^{-1}$; $S = 26.0 \pm 0.3$) released at a pressure of 550 Torr from a second pulsed valve operating at a pulse amplitude of -400 V and an opening time of $80 \mu\text{s}$; the secondary valve was triggered $35 \mu\text{s}$ prior to the primary pulsed valve. This resulted in a collision energy of $46.0 \pm 1.0 \text{ kJ mol}^{-1}$ and $50.0 \pm 1.0 \text{ kJ mol}^{-1}$, and center-of-mass angles of $13.1 \pm 0.3^\circ$ and $12.9 \pm 0.3^\circ$ for the $\text{C}_7\text{H}_7\text{Cl}$ and $\text{C}_7\text{D}_7\text{Cl}$ beams, respectively. The reactively scattered products were monitored using a triply differentially pumped quadrupole mass spectrometric detector in the time-of-flight (TOF) mode after electron-impact ionization of the neutral species with an electron energy of 80 eV. Time-of-flight spectra were recorded over the full angular range of the reaction in the plane defined by the primary and the secondary reactant beams. The TOF spectra were integrated and normalized to extract the product angular distribution in the laboratory frame (LAB). To extract information on the reaction dynamics, the experimental data is transformed into the center-of-mass frame utilizing a forward-convolution routine.^{30,31} This method initially assumes an angular flux distribution, $T(\theta)$, and the translational energy flux distribution, $P(E_T)$, in the center-of-mass system (CM). Laboratory TOF spectra and the laboratory angular distributions (LAB) are subsequently calculated from the $T(\theta)$ and $P(E_T)$ functions and compared to the experimental data, the functions are iteratively adjusted until the best fit between the two is achieved.

The synthesis of para-chlorotoluene-d7 started from commercially available para-toluidine. The starting material was deuterated using palladium–carbon (Pd/C) and platinum–carbon (Pt/C) catalysts and deuterium oxide in an autoclave at 190°C for 96 h. This deuteration procedure was

Scheme 2. Routes Employed to Synthesize Para-Chlorotoluene-d7



repeated three times to obtain the labeled compound. Deuteration progress was monitored with ^{13}C carbon NMR and mass spectrometry. Subsequently, the chloro compound was obtained by converting the toluidine to its diazonium salt and substitution of the diazo group with chloride in a Sandmeyer type reaction (Scheme 2 a).³² Synthesis starting from commercially available toluene-d7, as reported by Hashimoto,³³ proved to be less favorable due to a low overall yield (Scheme 2 b).

3. COMPUTATIONAL METHODS

Optimizations of geometries of the reactants, intermediates, transition states, and products were performed on the ground electronic state potential energy surface (PES) of $\text{C}_{11}\text{H}_{11}$ species for the reaction of para-tolyl radical with vinylacetylene, using the M06-2x density functional approach,^{34,35} with Dunning's correlation-consistent cc-pvtz basis set.^{36,37} For each optimized structure vibrational analysis was carried out at the same level and was used to characterize the nature (minimum or saddle) of the structure and to calculate zero-point energies (ZPE). Intrinsic reaction coordinate (IRC) was calculated from each transition state to identify the connected reactant and product. Single point energy was calculated at these optimized geometries using the coupled cluster CCSD-(T) method with the F12 correction^{38–40} with cc-pvdz basis set.^{36,37} The GAUSSIAN 09⁴¹ and MOLPRO 2012⁴² programs were employed for the calculations. The optimized Cartesian coordinates are given in Table S3 in the Supporting Information.

The energy-dependent rate constants for some individual reaction steps were computed using the microcanonical RRKM theory under single-collision conditions (zero-pressure limit).^{43–45} The rate constants were calculated both for reversible isomerization steps of $\text{C}_{11}\text{H}_{11}$ intermediates and for irreversible product formation steps. According to the RRKM theory, the rate constant $k(E)$ at an internal energy E for a unimolecular reaction $\text{A}^* \rightarrow \text{A}^\ddagger \rightarrow \text{P}$ can be expressed as^{43–45} $k(E) = [\sigma W^\ddagger(E-E^\ddagger)]/[h \rho(E)]$, where σ is the reaction path degeneracy, h is the Plank constant, $W^\ddagger(E-E^\ddagger)$ denotes the total number of states for the transition state (activated complex) A^\ddagger with a barrier E^\ddagger , $\rho(E)$ represents the density of states of the energized reactant molecule A^* having the energy E , and P are the products. The available internal energy E was taken as a sum of the potential energies of the para-tolyl radical plus vinylacetylene and the collision energy. The density of states was computed within the harmonic approximation. Once $k(E)$ was generated, it was utilized in the first-order kinetic equations according to the kinetic scheme incorporating all unimolecular reaction steps in the pertinent area of the $\text{C}_{11}\text{H}_{11}$ potential surface. These ordinary differential equations were then solved using the steady-state approximation, and the solution gave branching ratios of various products as functions of the collision energy. The individual forward and reverse rate constants, along with product branching ratios are given in Tables S1 and S2 in the Supporting Information.

4. EXPERIMENTAL RESULT

In the reaction of para-tolyl (C_7H_7 ; 91 amu) with vinylacetylene (C_4H_4 ; 52 amu), a scattering signal was observed at a mass-to-charge ratio (m/z) of 142 ($\text{C}_{11}\text{H}_{10}^+$). These findings indicate the reaction proceeds through hydrogen atom emission in a para-tolyl radical/hydrogen atom exchange mechanism.

The reaction of the para-tolyl-d7 (C_7D_7 ; 98 amu) radical with vinylacetylene was conducted under identical conditions as the hydrogenated para-tolyl vinylacetylene reaction to quantify to what extent the hydrogen atom originates from the vinylacetylene reactant. We observed a reactive scattering signal at $m/z = 149$ ($\text{C}_{11}\text{H}_3\text{D}_7$) indicating that, in the reaction of the para-tolyl-d7 (C_7D_7) with vinylacetylene (C_4H_4), the hydrogen atom is released from the vinylacetylene reactant. Note that scattering products were also observed at $m/z = 141$ ($\text{C}_{11}\text{H}_9^+$) and 140 ($\text{C}_{11}\text{H}_8^+$) in the reaction with the tolyl radical and at $m/z = 148$ ($\text{C}_{11}\text{H}_2\text{D}_7^+$) and 147 ($\text{C}_{11}\text{HD}_7^+/\text{C}_{11}\text{H}_2\text{D}_6^+$) in the experiment with the para-tolyl-d7 radical. These products had identical TOF profiles to the hydrogen atom loss products, $m/z = 142$ ($\text{C}_{11}\text{H}_{10}^+$) and $m/z = 149$ ($\text{C}_{11}\text{H}_3\text{D}_7^+$), respectively, and therefore were assigned to dissociative electron impact ionization of the products in the ionizer.

Figure 1 depicts selected time-of-flight (TOF) spectra recorded at $m/z = 142$ ($\text{C}_{11}\text{H}_{10}$) (A) and at $m/z = 149$

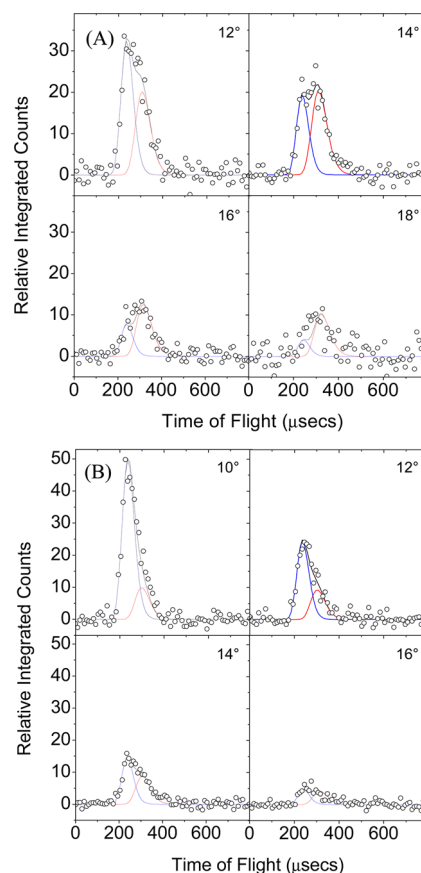


Figure 1. Time-of-flight data at various laboratory angles: (A) in the reaction of para-tolyl radicals (C_7H_7) with vinylacetylene (C_4H_4) at a collision energy of 46 kJ mol^{-1} obtained at $m/z = 142$, (B) in the reaction of para-tolyl-d7 radicals (C_7D_7) with vinylacetylene (C_4H_4) at a collision energy of 50 kJ mol^{-1} obtained at $m/z = 149$. Circles and error bars indicate experimental data, and the blue and red lines represent the fits derived from nonreactive and reactive channels respectively, whereas the black line presents the sum.

($\text{C}_{11}\text{H}_3\text{D}_7$) (B). These data had to be fit with two channels associated with nonreactive (fast) and reactive (slow) scattering signal. The reactive scattering signal (red line) is indicative of the synthesis of a product with the molecular formula $\text{C}_{11}\text{H}_{10}$ and $\text{C}_{11}\text{H}_3\text{D}_7$ formed through addition of para-tolyl radical to

vinylacetylene accompanied with dissociation of a hydrogen atom. The laboratory angular distribution of this channel, shown in Figure 2, is symmetric around the center-of-mass

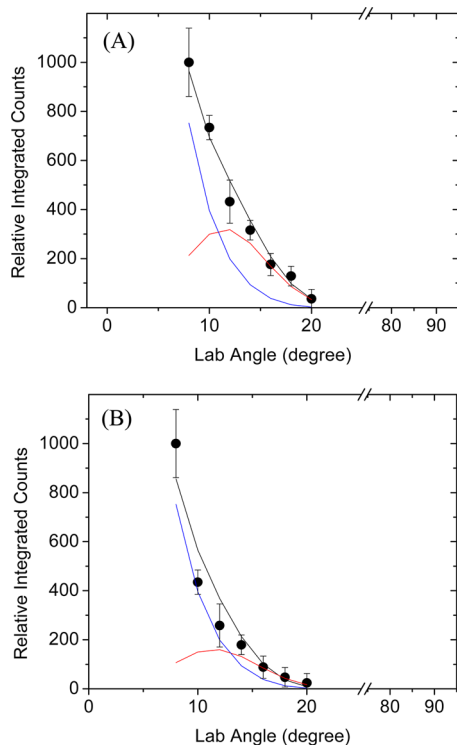


Figure 2. Laboratory angular distribution (LAB): (A) in the reaction of para-tolyl radicals (C_7H_7) with vinylacetylene (C_4H_4) at a collision energy of 46 kJ mol^{-1} obtained at $m/z = 142$, (B) in the reaction of d7-para-tolyl radicals (C_7D_7) with vinylacetylene (C_4H_4) at a collision energy of 50 kJ mol^{-1} obtained at $m/z = 149$. Circles and error bars indicate experimental data, and the blue and red lines represent the fits derived from nonreactive and reactive channels respectively, whereas the black line presents the sum.

angle of $13.1 \pm 0.3^\circ$ and $12.9 \pm 0.3^\circ$ proposing indirect scattering dynamics via complex formation ($C_{11}H_{11}/C_{11}H_4D_7$). The nonreactive scattering signal (blue lines Figure 1 and 2) at $m/z = 142$ to 140 in the hydrogenated tolyl experiments and at $m/z = 148$ to 146 in the deuterated tolyl experiments is caused by a contaminant in the primary beam due to purity of the starting material being only 98%. Here, the part of the laboratory angular distribution of the nonreactive scattering signal can be nicely reproduced by replacing the argon-seeded vinylacetylene beam by a pure argon beam, showing a steady decay in scattering signal as the laboratory angle increases.

Having established the formation of a molecule with the molecular formula $C_{11}H_{10}$ (142 amu) and $C_{11}H_3D_7$ (149 amu), we attempt now to elucidate the underlying reaction dynamics by converting the laboratory data into the center-of-mass frame. Fundamentally both the fully hydrogenated and partially deuterated tolyl plus vinylacetylene reactions could be fit with the same center-of-mass functions: the center-of-mass translational energy ($P(E_T)$) and angular ($T(\theta)$) distributions displayed in Figure 3. The center-of-mass translational energy distribution depicts a maximum translational energy release of $306 \pm 30 \text{ kJ mol}^{-1}$. By subtracting the collision energy of 46 kJ mol^{-1} and 50 kJ mol^{-1} , we obtain the reaction exoergicities of $260 \pm 30 \text{ kJ mol}^{-1}$ in forming $C_{11}H_{10}$ isomers plus atomic

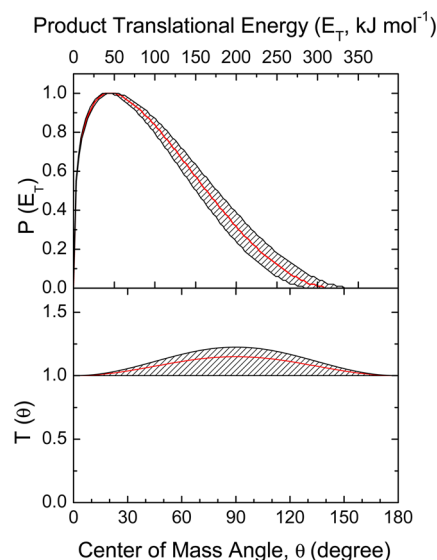


Figure 3. Center-of-mass translational energy distribution (top) and angular distribution (bottom) for the reaction of para-tolyl radicals (C_7H_7) with vinylacetylene (C_4H_4) to form 2-methylnaphthalene ($C_{10}H_7CH_3$) plus atomic hydrogen at a collision energy of 46 kJ mol^{-1} , and in the reaction of d7-para-tolyl radicals (C_7D_7) with vinylacetylene (C_4H_4) at a collision energy of 50 kJ mol^{-1} obtained at $m/z = 149$.

hydrogen and $256 \pm 30 \text{ kJ mol}^{-1}$ in forming $C_{11}H_3D_7$ isomers plus atomic hydrogen, for those products formed without internal excitation. Actually, the center-of-mass translational energy distribution $P(E_T)$ shows a pronounced peaking at about $35\text{--}55 \text{ kJ mol}^{-1}$, and the average amount of energy released into the translational degrees of freedom of the products is $99 \pm 20 \text{ kJ mol}^{-1}$, i.e., $32 \pm 6\%$ of the total available energy, indicating that at least one reaction channel to form the $C_{11}H_{10}/C_{11}H_3D_7$ isomer(s) plus atomic hydrogen holds a tight exit transition state with a repulsive carbon–hydrogen bond rupture. Note that the center-of-mass angular distribution $T(\theta)$ shows a broad intensity distribution over the whole angular range. This distribution is forward–backward symmetric with respect to 90° , indicating an indirect, complex-forming reaction mechanism involving $C_{11}H_{11}/C_{11}H_4D_7$ intermediate(s).⁴⁶ The forward–backward symmetry of $T(\theta)$ implies a lifetime of the decomposing complex(es) being longer than its rotational period.⁴⁷ Lastly, the center-of-mass angular distribution, $T(\theta)$, is moderately peaked at 90° . This finding indicates that the decomposing $C_{11}H_{11}/C_{11}H_4D_7$ intermediate emits the hydrogen atom almost perpendicularly to the rotational plane of the decomposing intermediate nearly parallel to the total angular momentum vector. This “sideways” scattering is also seen in the flux contour map (Figure 4).

5. THEORETICAL POTENTIAL ENERGY PROFILES

All the reactions of para-tolyl radical ($C_6H_4CH_3$; X^2A_1) with vinylacetylene (X^1A') in the ground electronic state start with addition of para-tolyl radical to the carbon 1, 2, 3, and 4 of vinylacetylene, $C^1H_2=C^2H-C^3\equiv C^4H$. The potential energy profiles of the reactions initiating with these addition reactions are shown in Figures 5 to 8, respectively. Figure 5 shows the potential energy profile for the channel starting with addition at C^1 , the terminal vinyl carbon. As shown in Figure S1 in the Supporting Information, a relaxed scan as a function of the C^1-C^{para} distance initially gives a weak initial van der Waals

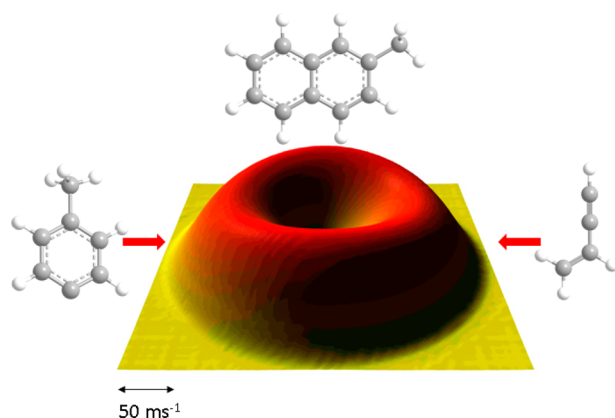


Figure 4. Flux contour map for the reaction of para-tolyl radical (C_7H_7) with vinylacetylene (C_4H_4) leading to 2-methylnaphthalene ($C_{11}H_{10}$) and atomic hydrogen.

complex at around 2.4 Å with the relative energy (with respect to the reactants) of about 5 kJ mol^{-1} below the separated reactants followed by a small barrier of only 1 kJ mol^{-1} at around 2.25 Å, before reaching a stable intermediate 1 at -196 kJ mol^{-1} with deuterium atoms on the para-tolyl fragment. As will be seen later, the fact that this reaction occurs without barrier distinguishes this channel from the other three channels, all of which have a barrier. The intermediate 1 can emit a hydrogen atom to give 1-para-tolyl-vinylacetylene product, with the transition state (TS) at -20 kJ mol^{-1} . However, a lower energy pathway via several intermediates exists to give 2-methylnaphthalene plus atomic hydrogen. In this pathway, the vinyl radical carbon internally abstracts a deuterium atom from

the 3 position of the tolyl group to produce a rather unstable intermediate 2 via TS 1-2 at -43 kJ mol^{-1} , which then cyclizes at the 4-position to form a very stable cyclic radical intermediate 3 via a relatively low TS 2-3 at -72 kJ mol^{-1} . Some intermediates, such as 2, may have *cis* or *trans* isomers; however, in the present paper, in order to focus on the reaction mechanism, we did not attempt to distinguish between *cis* and *trans* isomers in any intermediate. The intermediate 3 goes over a large barrier 3-4 at -93 kJ mol^{-1} , consisting of a transfer of a hydrogen atom from C^2 to C^3 , and produces the most stable π radical intermediate 4. Alternatively, a deuterium atom can transfer from C^2 to C^3 via transition state 3-4' at -90 kJ mol^{-1} , leading to intermediate 4'. If there is any collision partner to dissipate excess internal energy or any reactive partner to react with them, 3, 4, or 4', their derivatives would be trapped and observable. With no collision partner, 4 and 4' can emit a hydrogen atom via a low energy tight TS 4-h and 4-h' to provide the very stable product, a partially deuterated 2-methylnaphthalene. In addition to this path leading to a bicyclic aromatic, there is a path leading to 1-para-tolyl-vinylacetylene by dissociation of a hydrogen atom from the initial stable intermediate 1 via TS 1-h.

Figure 6 gives the potential energy profile for the channel starting with addition of para-tolyl radical to the terminal acetylene carbon C^4 . As discussed above, we ignore a weak van der Waals complex that does not affect the kinetics in this as well as in the other channels. The initial addition to give intermediate 5 has a small but importantly positive barrier of 9 kJ mol^{-1} with deuterium atoms on the para-tolyl fragment at TS 0-5. As in the C^1 channel, the intermediate 5 can eject a hydrogen atom via a high TS 5-h at -30 kJ mol^{-1} with

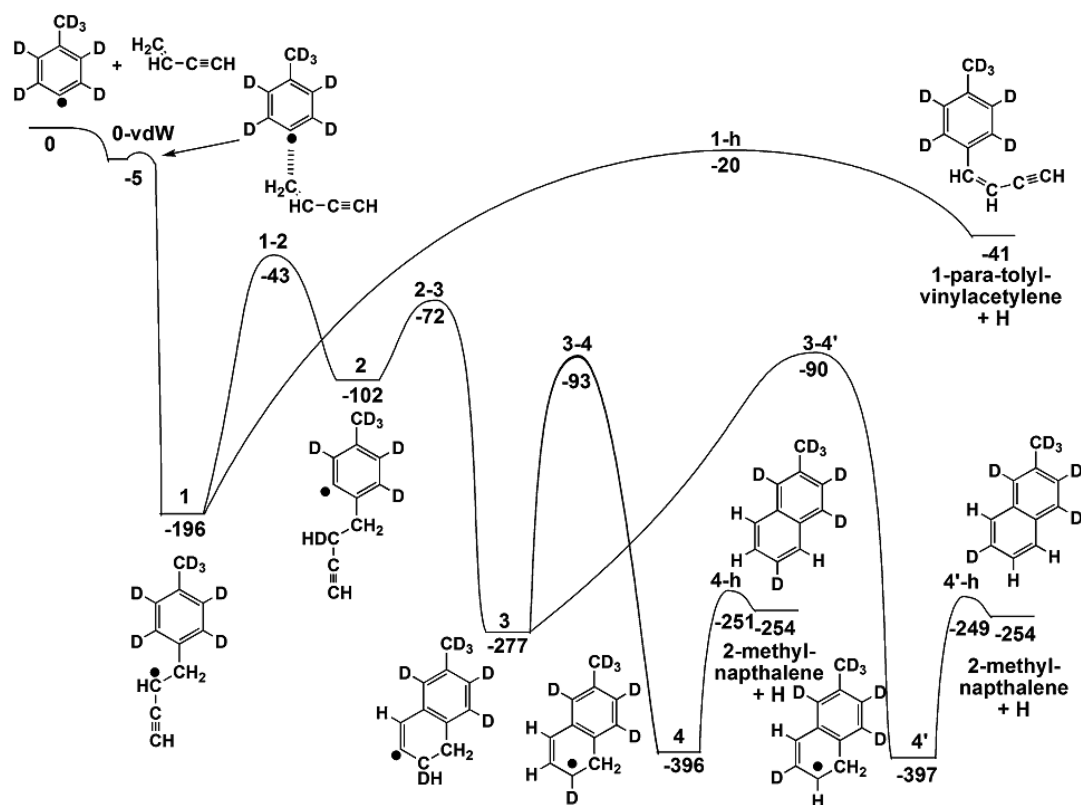


Figure 5. Potential energy profile of C^1 addition channel surface (PES) in the reaction of the deuterated para-tolyl radical with vinylacetylene. Relative energies in kJ mol^{-1} are the E(CCSD(T)-F12/cc-pvdz//M06-2x/cc-pvtz + ZPE(M06-2x/cc-pvtz) level.

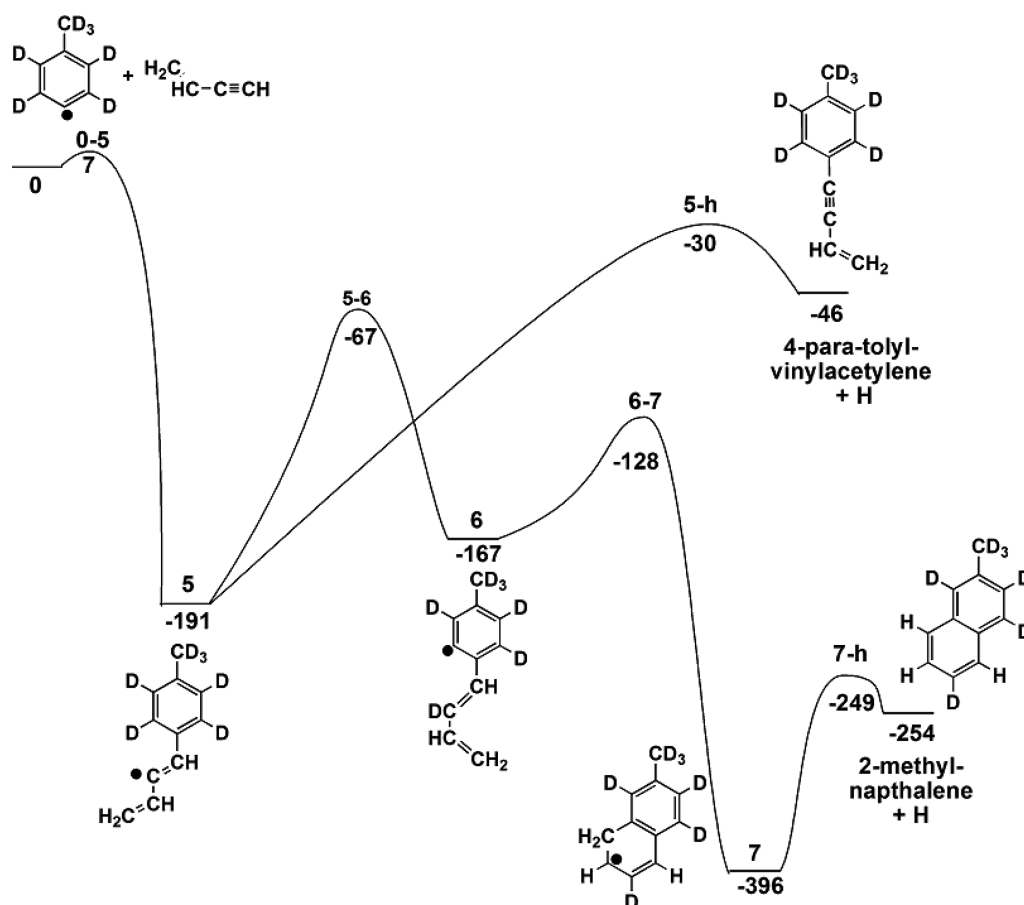


Figure 6. Potential energy profile of C^4 addition channel surface (PES) in the reaction of the deuterated para-tolyl radical with vinylacetylene. Relative energies in kJ mol^{-1} are the E(CCSD(T)-F12/cc-pvdz//M06-2x/cc-pvtz + ZPE(M06-2x/cc-pvtz) level.

deuterium atoms on the para-tolyl fragment, to give a partially deuterated 4-para-tolyl-vinylacetylene product. More favorable is the pathway with several intermediates, which starts with an internal abstraction of atomic hydrogen from the tolyl radical to give a σ radical intermediate **6**, followed by cyclization to give a stable π radical intermediate **7**, which could be trapped with a collision or reaction partner. Otherwise, **7** loses a hydrogen atom to give 2-methylnaphthalene, the same product as in the C^1 channel.

Figure 7 shows the potential energy profile for the channel starting with addition of para-tolyl radical to the acetylene internal carbon C^3 . This addition requires a barrier of 13 kJ mol^{-1} with deuterium atoms on the para-tolyl fragment at TS **0-8**. Intermediate **8** has to go through cyclization to give a three-membered ring compound **9** and reopening to get to intermediate **10**. Intermediate **10** can directly expel a hydrogen atom to give a partially deuterated 4-para-tolyl-vinylacetylene product, with the transition state (TS) at -25 kJ mol^{-1} . A better pathway for **10** is to go through hydrogen abstraction from the tolyl ring to give **11**, followed by cyclization and reopening to provide an intermediate **13**, which cyclizes to give a stable bicyclic intermediate **14**. Intermediate **14** may be trapped with collision or reaction partner, but without partner, it will eliminate a hydrogen atom to produce 2-methylnaphthalene, the same product as in C^1 and C^4 channels.

Figure 8 presents the potential energy profile for the channel starting with addition of the para-tolyl radical to the vinyl internal carbon C^2 . The initial addition reaction to provide an intermediate **15** has a barrier of 6 kJ mol^{-1} at TS **0-15**.

Intermediate **15** goes through cyclization to a three-membered ring intermediate **16**, which reopens easily to give an intermediate **17**. Intermediate **17** may be observable if it is trapped by collision or reaction. With no collision, it will eliminate a hydrogen atom via a TS **17-h** of -24 kJ mol^{-1} , to form a partially deuterated 1-para-tolyl-vinylacetylene product.

In addition, there are possibilities of para-tolyl radical to abstract a hydrogen atom from vinylacetylene. As shown in Figure S2 in the Supporting Information, however, the abstraction of a hydrogen atom from the vinyl C^1 and C^2 atoms to produce toluene and *n*- and *i*- C_4H_3 radicals has high barriers of 33 kJ mol^{-1} and 15 kJ mol^{-1} , respectively.

6. COMPARISON BETWEEN EXPERIMENT AND COMPUTATION

Now we compare the results from the electronic structure calculations with the crossed molecular beam data in an attempt to rationalize the product(s) formed and to elucidate the underlying reaction mechanism. First, let us compare the experimentally determined reaction energy of $260 \pm 30 \text{ kJ mol}^{-1}$ to form $C_{11}H_{10}$ isomer(s) plus atomic hydrogen with the computed data. The computations predict that the formation of 2-methylnaphthalene ($C_{10}H_7CH_3$) is associated with a reaction exoergicity of $261 \pm 8 \text{ kJ mol}^{-1}$ (Figures 5–8). These experimental and theoretical results agree very well, and we can conclude that 2-methylnaphthalene is formed in the reaction of the para-tolyl radical with vinylacetylene. The computations also predict the formation of two partially deuterated non-

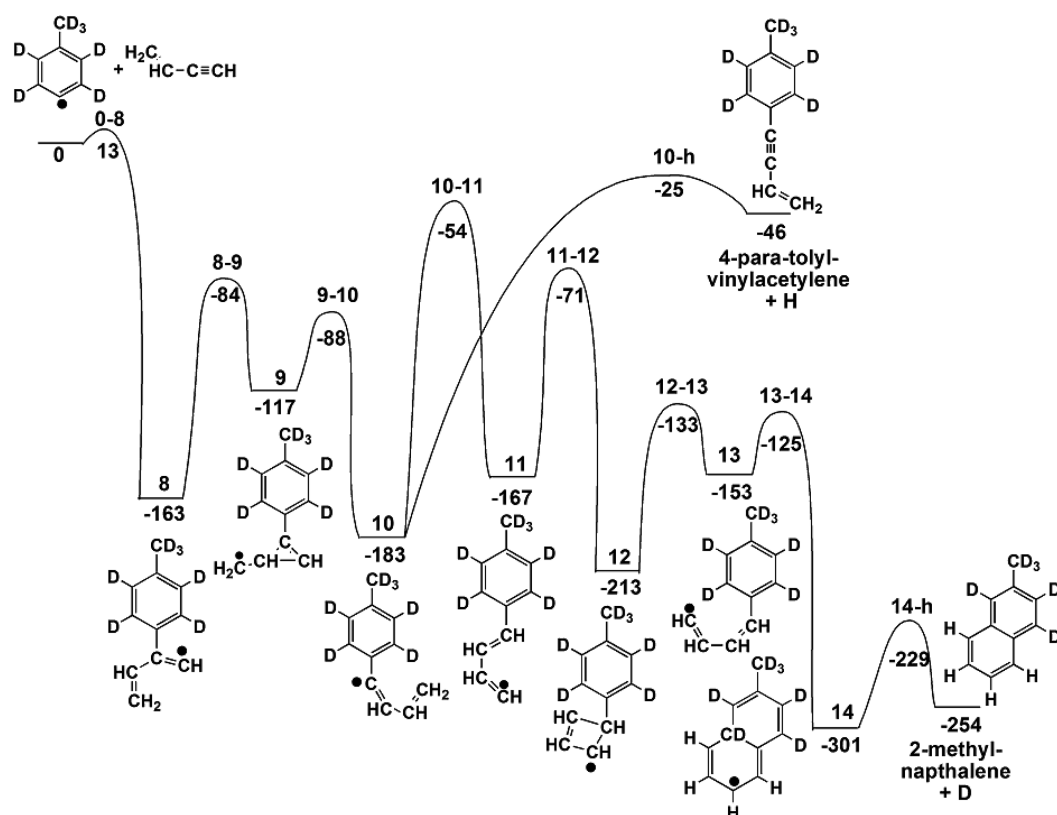


Figure 7. Potential energy profile of C^3 addition channel surface (PES) in the reaction of the deuterated para-tolyl radical with vinylacetylene. Relative energies in kJ mol^{-1} are the E(CCSD(T)-F12/cc-pvdz//M06-2x/cc-pvtz + ZPE(M06-2x/cc-pvtz) level.

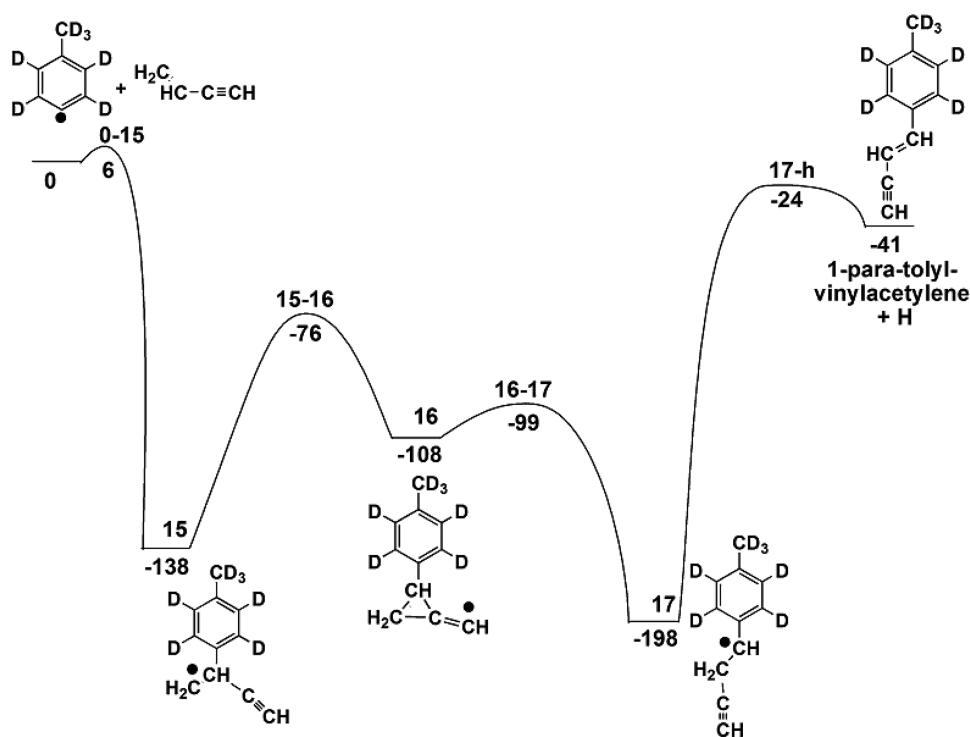


Figure 8. Potential energy profile of C^2 addition channel surface (PES) in the reaction of the deuterated para-tolyl radical with vinylacetylene. Relative energies in kJ mol^{-1} are the E(CCSD(T)-F12/cc-pvdz//M06-2x/cc-pvtz + ZPE(M06-2x/cc-pvtz) level.

naphthalene isomers, 4-para-tolyl-vinylacetylene with an exoergicity of $46 \pm 8 \text{ kJ mol}^{-1}$, shown in Figures 6 and 7, and 1-para-tolyl-vinylacetylene with an exoergicity of $41 \pm 8 \text{ kJ}$

mol^{-1} , shown in Figures 5 and 8. These monocyclic isomers can be formed via initial addition of the para-tolyl radical to the radical center at the C^1 , C^2 , C^3 , and C^4 carbon atoms of

vinylacetylene, yielding the initial intermediates **1**, **8**, **15**, and **5**, respectively, which undergo either isomerization prior to cyclization and atomic hydrogen loss to form 2-methylnaphthalene, with overall lower barriers, or unimolecular decomposition with higher barriers via atomic hydrogen loss to form monocyclic isomers. Although monocyclic products were not observed in the present experiment, by considering their reaction energies and integrating the center-of-mass translational energy distribution, we can predict upper limits of these isomers to be about 30%.⁴⁸

Having identified 2-methylnaphthalene as the major reaction product, we now elucidate the underlying reaction mechanism(s) for its formation. The calculations propose three feasible entrance channels (Figures 5, 7, and 6), in which the para-tolyl radical adds with its radical center to the C¹, C³, and C⁴ carbon atoms of the vinylacetylene reactant leading to intermediates **1**, **8**, and **5** that are bound by 196, 163, and 191 kJ mol⁻¹, respectively. It is important to stress that the addition at the C¹ position forms a van der Waals complex 6 kJ mol⁻¹ below the reactant energy and goes over a *submerged barrier* located at -5 kJ mol⁻¹, at a long R(C_{paratolyl}-C¹) bond distance (Figure 5). This in effect *has no entrance barrier*. In contrast, additions to C³ and C⁴ have entrance barriers of 13 and 7 kJ mol⁻¹, respectively. Considering our collision energy of 46.0 ± 1.0 kJ mol⁻¹ and 50.0 ± 1.0 kJ mol⁻¹, all three entrance channels are open. As explained in detail in the preceding section, these initial adducts **1**, **8**, and **5** undergo a variety of isomerization processes including hydrogen migration, ring closure, ring-opening and eventually leading to intermediates **4**, **14**, and **7**, with energies of -396, -301, and -396 kJ mol⁻¹, relative to the reactants. All three intermediates can lose a hydrogen atom producing the final product, 2-methylnaphthalene, through tight exit transition states. Recall that the existence of an exit transition state was proposed experimentally based on the off-zero peaking of the center-of-mass translational energy distribution. Furthermore, the sideways scattering and preferential emission of the hydrogen atom perpendicularly to the rotational plane of the decomposing complex and hence parallel to the total angular momentum vector as observed in the experimental center-of-mass angular distribution can be also verified from the structures of the exit transition states. As shown in Figure 9, at the final hydrogen loss transition states, **4-h**, **14-h**, and **7-h**, the leaving hydrogen atom has dihedral angles of 78.3°, 78.4°, and 88.5°, respectively, relative to the plane of the aromatic ring and the exiting hydrogen atom, in close agreement with our experimental findings.

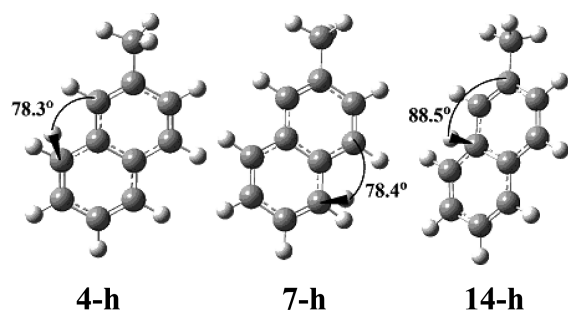


Figure 9. Computed dihedral angle between the molecular plane of the nascent 2-methylnaphthalene and ejecting H atom in the transition state from the intermediates of **4**, **7**, and **14**, respectively.

In considering three available reaction pathways to the observed 2-methylnaphthalene product beginning with addition to C¹, C³ and C⁴ carbons, which is the dominant route? From the reactions of d7-tolyl plus vinylacetylene we find that an atomic hydrogen loss is observed. Considering the experimental (TOFs and angular distribution) and center-of-mass functions (translational energy ($P(E_T)$) and angular ($T(\theta)$) distributions) are identical in both para-tolyl-vinylacetylene and d7-para-tolyl-vinylacetylene reactions, we can state that 2-methylnaphthalene is formed through light atom emission from a reaction pathway involving light atom emission from vinylacetylene only. If we analyze the reaction pathways through additions to C¹, C³, and C⁴ carbons as shown in Figures 5, 7, and 6, respectively, we see that addition to C³ results in deuterium emission only. Therefore, at our collision energy of 46 kJ mol⁻¹ and 50.0 ± 1.0 kJ mol⁻¹, we find that the reaction route initiated through addition to C³ is closed. The reaction route through C³ addition also has an unfavorable entrance barrier of 14 kJ mol⁻¹. Furthermore, from the initial collision complexes **1**, **8**, and **5**, intermediate **8** requires six isomerization steps compared to three and two for intermediates **1** and **5**, respectively, to reach the pre-hydrogen-loss complexes. The two reaction pathways that are open to reach 2-methylnaphthalene are shown in Figures 5 and 6, representing addition to the C¹ and C⁴ carbons, respectively, but which one is the most dominant? A major difference between the two channels is that the addition of the tolyl radical to the C¹ carbon atom of vinylacetylene is barrierless, thus providing an “easier” route compared to the competing addition to C⁴, which has an associated entrance barrier. It should be noted, both these reaction pathways are open in combustion relevant environments holding temperatures up to a few 1,000 K due to their low or nonexistent entrance barriers.

In summary, under present experimental conditions, both microchannels are open, but the addition to C¹ is barrierless and has a lower number of isomerization steps, suggesting that this pathway is the most preferred route. Consequently, in cold molecular clouds holding temperatures as low as 10 K, *only the barrierless addition to C¹ is open*. Therefore, in the interstellar medium and also in the low temperature, hydrocarbon-rich atmospheres of planets and their moons in the outer Solar System such as on Titan, the formation of 2-methylnaphthalene is facile through the path involving intermediate **1**. Furthermore, a previous crossed beam experiment investigating the reaction of phenyl radicals with vinylacetylene leading to naphthalene found through the exploitation of deuterated reactants that the phenyl radical preferentially adds at the C¹ position.²⁰ Note that in the present experiment, all addition pathways can also lead to monocyclic products 1-para-tolyl-vinylacetylene and 4-para-tolyl-vinylacetylene at levels of 30% at most compared to 2-methylnaphthalene.

Also, the branching ratios for the C¹ addition reaction pathway calculated via statistical methods (RRKM) predict that 2-methylnaphthalene is 98.8% of the product, while cis-1-para-tolyl-vinylacetylene accounts for the remaining 1.2% (Table S3 in the Supporting Information). The reaction channels leading to the other initial adducts, namely, para-tolyl addition to C², C³, and C⁴ of vinylacetylene, were not considered in our RRKM calculations. Addition of para-tolyl to C², C³, and C⁴ of vinylacetylene have entrance barriers leading to the initial adduct, while para-tolyl addition to C¹ of vinylacetylene has a submerged barrier and, in effect, is barrierless. The statistical RRKM theory is suitable for barrierless reaction channels only.

Finally, it is important to address reaction pathways involving the hydrogen abstraction from the C² and C¹ carbon atoms forming toluene and *i*-C₄H₃ and *n*-C₄H₃, respectively (Figure S2 in the Supporting Information). These hydrogen abstraction pathways have barriers of 20 and 35 kJ mol⁻¹, and are exoergic by 48 and 20 kJ mol⁻¹, respectively. These high entrance barriers imply that these pathways cannot compete in cold environments like in cold molecular clouds; however, they might be open in combustion flames.

7. CONCLUSIONS

We have conducted crossed molecular beam experiments of para-tolyl and para-tolyl-d7 radicals with vinylacetylene at collision energies of 46 kJ mol⁻¹ and 50 kJ mol⁻¹. These experiments were combined with electronic structure and RRKM calculations of the C₁₁H₁₁ potential energy surface. Our investigation provides evidence that a methyl-substituted PAH—2-methylnaphthalene—can be formed via indirect scattering dynamics through a bimolecular collision of a substituted aromatic radical—the para-tolyl radical and an acyclic hydrocarbon—vinylacetylene. The reaction is initiated by the addition of the para-tolyl radical to either the acetylenic (C⁴) or vinyl (C¹) carbons, leading eventually to two distinct doublet radical intermediates. Although both routes are open at our collision energy, only the addition at the vinyl group C¹ was found to be *barrierless*. This barrierless route to 2-methylnaphthalene has strong implications to extreme environments such as the interstellar medium and hydrocarbon-rich atmospheres of planets and their moons in the outer Solar System and provides a facile synthetic pathway to alkyl-substituted PAHs such as 2-methylnaphthalene in cold molecular clouds even at temperatures as low as 10 K potentially populating the interstellar medium with species responsible for the broad 3.4 μm feature in the UIEs. Finally, we show that the reaction of the para-tolyl radical with unsaturated hydrocarbons such as vinylacetylene can mechanistically arrive at methyl substituted PAHs under single collision conditions, and can provide a barrierless formation mechanism by which *odd-numbered* PAHs are formed in such quantities as found in combustion environments and meteorites.

■ ASSOCIATED CONTENT

■ Supporting Information

Experimental procedure, characterization NMR data, and figures of the van der Waals complex upon the addition of para-tolyl to the C¹ carbon atom of vinylacetylene as well as the hydrogen abstraction PES of vinylacetylene by para-tolyl. The RRKM rate constants and statistical branching ratios from para-tolyl addition to C¹ carbon atom of vinylacetylene are also given. The Cartesian coordinates of all the optimized structures are also tabulated. This material is available free of charge via the Internet at <http://pubs.acs.org>.

■ AUTHOR INFORMATION

Corresponding Authors

*E-mail: ralfk@hawaii.edu.

*E-mail: keiji.morokuma@emory.edu.

Notes

The authors declare no competing financial interest.

■ ACKNOWLEDGMENTS

This work was supported by the US Department of Energy, Basic Energy Sciences (DE-FG02-03ER15411), at University of Hawaii and also by the Air Force Office of Scientific Research (FA9550-10-1-0304 and FA9550-12-1-0472) at Emory University.

■ REFERENCES

- (1) Morgan, G. T.; Pratt, D. D. Complex aromatic hydrocarbons in low-temperature tar. *Nature* **1927**, *118*, 805–805.
- (2) Tian, Z.; Pitz, W. J.; Fournet, R.; Glaude, P. A.; Battin-Leclerc, F. A Detailed Kinetic Modeling Study Toluene Oxidation in a Premixed Flame. *Proc. Combust. Inst.* **2011**, *33*, 233–241.
- (3) Yang, B.; Li, Y.; Wei, L.; Huang, C.; Wang, J.; Tian, Z.; Yang, R.; Sheng, L.; Zhang, Y.; Qi, F. An experimental study of the premixed benzene/oxygen/argon flame with tunable synchrotron photoionization. *Proc. Combust. Inst.* **2007**, *31*, 555–563.
- (4) Li, Y.; Zhang, L.; Tian, Z.; Yuan, T.; Wang, J.; Yang, B.; Qi, F. Experimental Study of a Fuel-Rich Premixed Toluene Flame at Low Pressure. *Energy Fuels* **2009**, *23*, 1473–1485.
- (5) Huang, C.; Wei, L.; Yang, B.; Wang, J.; Li, Y.; Sheng, L.; Zhang, Y.; Qi, F. Lean Premixed Gasoline/Oxygen Flame Studied with Tuneable Synchrotron Vacuum UV Photoionization. *Energy Fuels* **2006**, *20*, 1505–1513.
- (6) Olten, N.; Senkan, S. M. Formation of Polycyclic Aromatic Hydrocarbons in an Atmospheric Pressure Ethylene Diffusion Flame. *Combust. Flame* **1999**, *118*, 500–507.
- (7) Finlayson-Pitts, B. J.; Pitts, J. N., Jr. Tropospheric air pollution: ozone, airborne toxics, polycyclic aromatic hydrocarbons, and particles. *Science* **1997**, *276*, 1045–1052.
- (8) Baird, W. M.; Hooven, L. A.; Mahadevan, B. Carcinogenic polycyclic aromatic hydrocarbon-DNA adducts and mechanism of action. *Environ. Mol. Mut.* **2005**, *45*, 106–114.
- (9) Duley, W. W. Polycyclic aromatic hydrocarbons, carbon nanoparticles and the diffuse interstellar bands. *Faraday Discuss.* **2006**, *133*, 415–425.
- (10) Salama, F.; Galazutdinov, G. A.; Krelowski, J.; Allamandola, L. J.; Musaev, F. A. Polycyclic aromatic hydrocarbons and the diffuse interstellar bands. A survey. *Astrophys. J.* **1999**, *526*, 265–273.
- (11) Ricks, A. M.; Douberly, G. E.; Duncan, M. A. The infrared spectrum of protonated naphthalene and its relevance for the unidentified infrared bands. *Astrophys. J.* **2009**, *702*, 301–306.
- (12) Kwok, S.; Zhang, Y. Mixed aromatic–aliphatic organic nanoparticles as carriers of unidentified infrared emission features. *Nature* **2011**, *479*, 80–83.
- (13) Li, A.; Draine, B. T. The Carriers of the Interstellar Unidentified Infrared Emission Features: Aromatic or Aliphatic? *Astrophys. J.* **2012**, *760*, L31–L35.
- (14) Geballe, T. B.; Tielens, A. G. G. M.; Kwok, S.; Hrivnak, B. J. Unusual 3 micron emission features in three proto-planetary nebulae. *Astrophys. J.* **1992**, *387*, L89–L91.
- (15) Hrivnak, B. J.; Geballe, T. B.; Kwok, S. A Study of the 3.3 and 3.4 μm Emission Features in Protoplanetary Nebulae. *Astrophys. J.* **2007**, *662*, 1059–1066.
- (16) Pendleton, Y. J.; Sandford, S. A.; Allamandola, L. J.; Tielens, A. G. G. M.; Sellgren, K. Near-Infrared absorption spectroscopy of interstellar hydrocarbon grains. *Astrophys. J.* **1994**, *437*, 683–696.
- (17) Eilsila, J. E.; De Leon, N. P.; Buseck, P. R.; Zare, R. N. Alkylation of polycyclic aromatic hydrocarbons in carbonaceous chondrites. *Geochim. Cosmochim. Acta* **2005**, *69*, 1349–1357.
- (18) Spencer, M. K.; Hammond, M. R.; Zare, R. N. Laser mass spectrometric detection of extraterrestrial aromatic molecules: mini-review and examination of pulsed heating effects. *Proc. Natl. Acad. Sci. U.S.A.* **2008**, *105*, 18096–18101, S18096/1–S18096/9.
- (19) Sephton, M. A. Organic compounds in carbonaceous meteorites. *Nat. Prod. Rep.* **2002**, *19*, 292–311.
- (20) Parker, D. S. N.; Zhang, F.; Kim, Y. S.; Kaiser, R. I.; Landera, A.; Kislov, V. V.; Mebel, A. M.; Tielens, A. G. G. M. Low Temperature

Formation of Naphthalene and its Role in the Synthesis of PAHs (Polycyclic Aromatic Hydrocarbons) in the Interstellar Medium. *Proc. Natl. Acad. Sci. U.S.A.* **2012**, *109*, 53–58.

(21) Kislov, V. V.; Islamova, N. I.; Kolker, A. M.; Lin, S. H.; Mebel, A. M. Hydrogen Abstraction Acetylene Addition and Diels-Alder Mechanisms of PAH Formation: A Detailed Study Using First Principles Calculations. *J. Chem. Theory Comput.* **2005**, *1*, 908–924.

(22) Frenklach, M.; Wang, H. Detailed Modeling of Soot Particle Nucleation and Growth. *Proc. Combust. Inst.* **1991**, *23*, 1559.

(23) Bittner, J. D.; Howard, J. B. Composition profiles and reaction mechanisms in a near-sooting premixed benzene/oxygen/argon flame. *Symp. (Int.) Combust., [Proc.]* **1981**, *18th*, 1105–1116.

(24) Mebel, A. M.; Kislov, V. V. Can the $C_5H_5 + C_5H_5 \rightarrow C_{10}H_{10} \rightarrow C_{10}H_9 + H/C_{10}H_8 + H_2$ Reaction Produce Naphthalene? An Ab Initio/RRKM Study. *J. Phys. Chem. A* **2009**, *113*, 9825–9833.

(25) McEnally, C. S.; Pfefferle, L. D. The effects of slight premixing on fuel decomposition and hydrocarbon growth in benzene-doped methane nonpremixed flames. *Combust. Flame* **2002**, *129*, 305–323.

(26) Moriarty, N. W.; Frenklach, M. Ab initio study of naphthalene formation by addition of vinylacetylene to phenyl. *Proc. Combust. Inst.* **2000**, *28*, 2563–2568.

(27) Comandini, A.; Brezinsky, K. Theoretical Study of the Formation of Naphthalene from the Radical - Bond Addition between Single-Ring Aromatic Hydrocarbons. *J. Phys. Chem. A* **2011**, *115*, 5547–5559.

(28) Kaiser, R. I.; Maksyutenko, P.; Ennis, C.; Zhang, F.; Gu, X.; Krishtal, S. P.; Mebel, A. M.; Kostko, O.; Ahmed, M. Untangling the chemical evolution of Titan's atmosphere and surface-from homogeneous to heterogeneous chemistry. *Faraday Discuss.* **2010**, *147*, 429–478.

(29) Dames, E.; Wang, H. Isomerization kinetics of benzylic and methylphenyl type radicals in single-ring aromatics. *Proc. Combust. Inst.* **2013**, *34*, 307–314.

(30) Vernon, M. Ph.D. Thesis, University of California, Berkeley, Berkeley, CA, 1981.

(31) Weiss, M. S. Ph.D. Thesis, University of California, Berkeley, Berkeley, CA, 1986.

(32) Kochi, J. K. The Mechanism of the Sandmeyer and Meerwein Reactions. *J. Am. Chem. Soc.* **1957**, *79*, 2942–2948.

(33) Hashimoto, S. I.; Takahashi, S. Synthesis of deuterium-labelled peptido-aminobenzophenone [4-chloro-2-(2'-chlorobenzoyl)-N-(glycylglycyl)-N-methyl-anilide] and its metabolites. *J. Labelled Compd. Radiopharm.* **1982**, *19*, 867–880.

(34) Zhao, Y.; Truhlar, D. *Theor. Chem. Acc.* **2008**, *120*, 215–241.

(35) Papajak, E.; Leverentz, H.; Zheng, J.; Truhlar, D. G. Efficient Diffuse Basis Sets: cc-pVxZ+ and maug-cc-pVxZ. *J. Chem. Theory Comput.* **2009**, *5*, 1197–1202.

(36) Dunning, T. H., Jr. Gaussian basis sets for use in correlated molecular calculations. I. The atoms boron through neon and hydrogen. *J. Chem. Phys.* **1989**, *90*, 1007–23.

(37) Dunning, T.; Peterson, K.; Wilson, A. *J. Chem. Phys.* **2001**, *114*, 9244–9253.

(38) Purvis, G. D., III; Bartlett, R. J. A full coupled-cluster singles and doubles model: the inclusion of disconnected triples. *J. Chem. Phys.* **1982**, *76*, 1910–18.

(39) Knizia, G.; Adler, T.; Werner, H. Simplified CCSD(T)-F12 methods: theory and benchmarks. *J. Chem. Phys.* **2009**, *130*, 054104.

(40) Thomas, J.; DeLeeuw, B.; Vacek, G.; Schaefer, H., III A systematic theoretical study of the harmonic vibrational frequencies for polyatomic molecules - The single, double, and perturbative triple excitation coupled-cluster (CCSD(T)) method. *J. Chem. Phys.* **1993**, *98*, 1336–1344.

(41) Frisch, M. J., et al. *Gaussian 09*; 2009.

(42) Werner, H.-J.; et al. *MOLPRO, version 2010*; 2010.

(43) Eyring, H.; Lin, S. H.; Lin, S. M. *Basic Chem. Kinet.* **1980**, 512.

(44) Robinson, P. J.; Holbrook, K. A. *Unimol. React.* **1972**, 400.

(45) Steinfeld, J.; Francisco, J.; Hase, W. *Chemical Kinetics and Dynamics*; 1982.

(46) Levine, R. D. *Molecular Reaction Dynamics*; 2005.

(47) Miller, W. B.; Safron, S. A.; Herschbach, D. R. Exchange reactions of alkali atoms with alkali halides: A collision complex mechanism. *Discuss. Faraday Soc.* **1967**, *44*, 108–122.

(48) We get these upper limit branching ratios by drawing a line from the value of the collision energy 46 kJ mol^{-1} plus the enthalpy of formation of the monocyclic isomer of interest $41 \text{ kJ mol}^{-1} = 87 \text{ kJ mol}^{-1}$. We integrate everything from 0 to 87 kJ mol^{-1} and compare to the total amount up to $0-306 \text{ kJ mol}^{-1}$, to give us 30% and 70%.